

Numerical simulation of ultracold plasmas

S. G. Kuzmin and T. M. O'Neil

Department of Physics, University of California at San Diego, La Jolla, California 92093

(Received 6 February 2002; accepted 5 June 2002)

In recent experiments ultracold plasmas were produced by photoionizing small clouds of laser cooled atoms. This paper presents the results of molecular dynamic simulations for the early time evolution of such plasmas. Contrary to earlier speculation, no evidence of strong electron–electron correlations is observed in the simulations even if the initial value of the coupling parameter ($\Gamma_e = e^2/akT_e$) is much larger than unity. As electron–electron correlations begin to develop, the correlation energy is released to heat the electrons, raising the electron temperature to the point where $\Gamma_e \sim 1$ and limiting further development of correlation. Further heating of the electrons occurs as a by-product of three-body recombination. When a model of laser cooling is added to the simulation, the formation of strong ion–ion correlation is observed. Contrary to earlier suggestion, the rate of three-body recombination is observed to be in reasonable agreement with the traditional formula, $R = 3.9 \times 10^{-9} \text{ s}^{-1} [n(\text{cm}^{-3})]^2 [T_e(\text{K})]^{-9/2}$, but care must be taken to use the correct temporally evolving temperature, T_e . The simulations are challenging because it is necessary to follow three-body recombination into weakly bound (high n quasiclassical) Rydberg states, and the time scale for such states is short compared to that for the plasma dynamics. This kind of problem was faced earlier in computational astrophysics when studying binary star formation in globular clusters and the simulation method used here is adapted from such studies. © 2002 American Institute of Physics. [DOI: 10.1063/1.1497166]

I. INTRODUCTION

In recent experiments,^{1–3} ultracold neutral plasmas were produced by abruptly photoionizing small clouds of laser cooled xenon atoms, carefully adjusting the energy of the ionizing photons to barely exceed the ionization potential. Electron temperatures as low as $T_e \approx 0.1$ K were reported. The ions inherited the even lower temperature of the laser cooled atoms ($T_i \approx 10$ mK). In closely related experiments,^{4–6} the cooled atoms were photoexcited to high- n Rydberg states, and an ultracold plasma resulted from collisional processes. Here, we focus on the plasmas that were produced directly by photoionization, since the initial conditions for the plasma state are well defined.

These novel plasmas present interesting challenges to theory. For example, it has been suggested that the initial low temperature of the plasmas implies strong correlation.¹ Also, there has been a worry that the traditional theory of three-body recombination is not applicable at the low temperatures of the plasmas.^{1,3} In contrast, we argue here that rapid intrinsic heating of the electrons raises the temperature to the point where strong correlation cannot develop and where the traditional theory of three-body recombination is approximately correct. These arguments are substantiated by molecular dynamics simulations of the early time plasma evolution. We also simulate a proposed experiment⁷ in which the ions that result from photoionization are themselves laser cooled, and in this simulation strong ion–ion correlation is observed.

At the low temperatures of these plasmas, three-body recombination is very rapid—much faster than radiative recombination.⁸ Three-body recombination proceeds through a sequence of collisions, with the recombination energy car-

ried off by an electron, rather than a photon. One can think of the process as the collisional approach to a state of thermal equilibrium, which is a neutral gas.

The rate of three-body recombination is controlled by a kinetic bottleneck⁸ at a binding energy of a few kT_e , where k is the Boltzmann constant and T_e is the electron temperature. For binding energies above the bottleneck, subsequent collisions typically reionize an electron–ion pair. However, occasionally a collision leaves a bound pair with energy below the bottleneck. Then subsequent collisions produce a cascade to ever deeper binding. Thus, a pair can be declared recombined when it passes below the bottleneck. The simulations follow many bound pairs as they cascade to energies below the bottleneck. Since the critical range of binding energies scales like kT_e and since kT_e is orders of magnitude smaller than the Rydberg energy, the essential physics can be captured by a classical molecular dynamics simulation.

The necessity of following the recombination into weakly bound (high- n) Rydberg states is the main challenge to the simulation. The difficulty is that the time scale for an electron orbit in such a state is much shorter than the time scale for the orbit of a typical unbound electron. In plasma simulations of this kind some authors have used two time scales: one for particles with near neighbors and another for the remaining particles.⁹ Another variant is to use piecewise analytic solutions for Kepler orbits. We prefer a treatment that does not make special assumptions about particles with near neighbors, but seamlessly encompasses the continuum of time scales required.

Fortunately, such a treatment was developed previously in computational studies of binary star formation in globular clusters. The binary stars are the analog of the high- n Ryd-

berg atoms and the cluster is the analog of the plasma cloud. We have adapted a code developed by Aarseth¹⁰ for the study of binary star formation.

The code is a molecular dynamics simulation in the sense that the force on a given particle from each of the other particles is calculated directly. Time integration is effected with a predictor corrector scheme using a fourth order polynomial fit to the orbit. The crucial feature is that the time step for each particle is adjusted independently depending on such factors as the rate of change of the acceleration. Thus, a bound electron can have a much shorter time step than a typical electron without slowing down the whole simulation. To keep all of the particles moving in near synchrony, the code advances next the time step for the particle that is furthest behind in absolute time. To evaluate the force on this particle, the other particle positions are extrapolated back in time to exact synchrony using the polynomial fit to the orbits.

As one would expect, there are interesting parallels between three-body recombination in these plasmas and binary star formation in clusters. We will see that a by-product of three-body recombination is heating of the unbound electrons and even production of suprathermal electrons that are ejected from the plasma. Likewise, binaries "harden" by giving kinetic energy to other stars through collisional interactions, sometimes ejecting stars at high velocity from the core of the cluster.¹¹ This heating mechanism is now thought to be the primary mechanism for supporting globular clusters against gravothermal contraction and core collapse.¹²

Two recent papers^{13,14} have provided a good theoretical description of the long term evolution of ultracold plasma clouds. Our work is complementary in that it focuses on the early time microscopic physics: the correlation physics and the cascade process of three-body recombination. The Aarseth simulation method is ideally suited to focus on this physics.

II. CORRELATION AND INITIAL HEATING

A. Theory background

For a plasma in thermal equilibrium, the strength of correlation is determined by the coupling parameter $\Gamma = e^2/akT$, where a is the Wigner-Seitz radius (i.e., $4\pi a^3 n/3 = 1$).¹⁵ We use cgs units throughout the paper. For the maximum density and lowest temperatures reported in the experiments [i.e., $n \approx 2 \times 10^9 \text{ cm}^{-3}$, $T_e \approx 0.1 \text{ K}$, and $T_i \approx 10 \mu\text{K}$], the electron coupling parameter has the value $\Gamma_e \approx 30$, and the ion coupling parameter is much larger. Thus, one might expect the low temperatures to be associated with strong correlation.

However, the plasma is not created in a state of thermal equilibrium. Before photoionization, the neutral atoms are uncorrelated, so immediately after photoionization ion-ion and electron-electron correlations are negligible. There may be some electron-ion correlation that remains as an artifact of the ionization process, but this is not a thermal equilibrium correlation. For example, there is no long range order.

Thermal equilibrium correlations can develop only through the action of Coulomb interactions as the plasma

evolves. However, as the electron correlations begin to develop, the correlation energy is released to the electron plasma as heat, and this limits the strength of correlation reached. To reach a correlation strength corresponding to $\Gamma_e \approx 1$, each electron picks up thermal energy $kT_e \approx e^2/a$. At this point the coupling parameter has the value

$$\Gamma_e = e^2/akT_e \approx (e^2/a)/(e^2/a) = 1,$$

so further development of correlation ceases. Even if the initial electron temperature were zero, corresponding formally to infinite Γ_e , strong correlation would not develop.

We hasten to add that the initial electron temperature would not be zero even if the energy of the ionizing photons exactly matched the ionization potential (for a single isolated atom). Because of the Coulomb fields from neighboring electrons and ions, the ionization potential for atoms in the plasma varies from atom to atom by an amount of order e^2/a , and this sets a minimum temperature of order $kT_e \sim e^2/a$.¹³ The picture is further complicated by the fact the ionization process takes place over a finite time. Typically, heating due to the release of correlation energy is occurring while the plasma is being created.

In the following we ignore these complications and consider simulations where the initial electron and ion temperatures (or more precisely, kinetic energies) are zero, corresponding formally to infinite initial values for Γ_e and Γ_i . This gives correlations the best opportunity to develop. The observed failure of strong correlations to develop then emerges as an intrinsic consequence of the dynamics. The release of correlation energy as heat limits the development of correlation.

The time scale for this electron dynamics is of order ω_{pe}^{-1} , where $\omega_{pe} = \sqrt{4\pi n e^2/m_e}$ is the electron plasma frequency. On a longer time scale (i.e., $\omega_{pi}^{-1} = \sqrt{m_i/m_e} \omega_{pe}^{-1}$), ion-ion correlations begin to develop and the released energy heats the ions limiting the effective ion-ion correlation strength.

Murillo¹⁶ considered ion heating by the release of correlation energy, but he treated the electrons as a dielectric fluid, and focused on the liberation of correlation energy for a system of Debye shielded ions. Unfortunately, this approach misses the electron heating that dominates the early stages of evolution, and the degree of shielding depends through the Debye length on electron temperature (see Sec. II C).

B. Simulation results

By using properly scaled length and time, the number of parameters that define a simulation was reduced to a minimum. Length was scaled by the Wigner-Seitz radius a and time by the inverse of the electron plasma frequency ω_{pe}^{-1} . With these scalings, the equations of motion were specified by three parameters: the mass ratio m_i/m_e , the number of electrons (which was equal to the number of ions) N , and a rounding parameter ε for the Coulomb potential. To avoid singularities, the Coulomb potential was rounded to the form,

$$1/\sqrt{|\mathbf{r}_1 - \mathbf{r}_2|^2/a^2 + \varepsilon^2}, \quad (1)$$

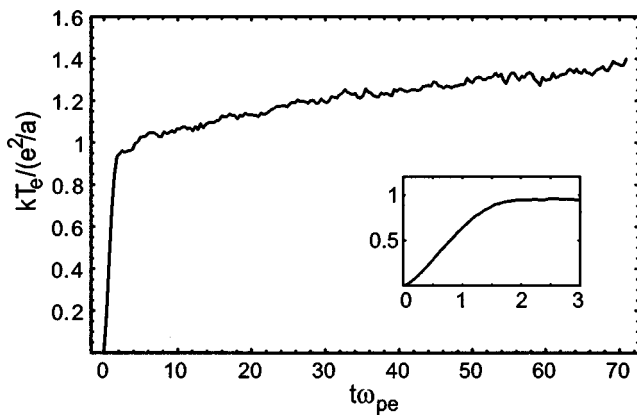


FIG. 1. Scaled temperature vs scaled time. The insert shows change of temperature during the time $t\omega_{pe} < 3$ when rapid heating occurs.

where $\varepsilon \ll 1$. For this simulation, ε was chosen to have the value $1/31$. This value is small enough that the rounded potential was a good approximation to the Coulomb potential for the vast majority of particles. For a few deeply bound pairs, the approximation was marginal, but these deeply bound pairs were not the focus of this simulation. The mass ratio was chosen to have the value $m_i/m_e = 100$. This relatively low value insured that the ions had time to participate in the correlation dynamics during the course of the simulation. The electron–electron correlation function relaxed to a steady-state form in a few scaled time units, and the ion–ion correlation function in a time that was longer by $\sqrt{m_i/m_e} = 10$. The simulation ran for $t_{\max}\omega_{pe} = 70.9$ scaled time units, and energy was conserved to an accuracy of $10^{-5}Ne^2/a$, where Ne^2/a is the scale of the total energy.

One might worry that the rapid heating is not resolved by the simulation since the heating occurs in about one unit of time (i.e., ω_{pe}^{-1}). However, the unit of time is not the time step. The time step is variable, but each particle has many time steps (typically hundreds) in one unit of time, so that the heating dynamics is adequately resolved.

So that the correlation function assumed the simple form $G(\mathbf{r}_1, \mathbf{r}_2) = G(|\mathbf{r}_1 - \mathbf{r}_2|)$, we arranged the initial and boundary conditions to insure uniform plasma density. Specifically, 4096 electrons and 4096 ions were distributed randomly inside a spherical volume bounded by a reflecting wall. The correlation measurements were made well away from the wall. In scaled units, the radius of the sphere was determined by the number of electrons, $(r_s/a)^3 = N$. As mentioned earlier, the initial temperatures for both electrons and ions were chosen to be zero.

The initial density profiles for the experimentally produced plasma clouds were Gaussian.^{1–3} One should think of the uniform density spherical plasmas as a small central section of a larger Gaussian cloud.

Figure 1 shows a plot of the scaled electron temperature [i.e., $kT_e(t)/(e^2/a) = 1/\Gamma_e(t)$] vs the scaled time $t\omega_{pe}$. To obtain this plot, histograms of electron kinetic energy were made (excluding tightly bound electrons) and matched to Maxwellians. Rapid heating to $\Gamma_e \approx 1$ is clearly visible. The longer-term slower heating is associated with three-body recombination.

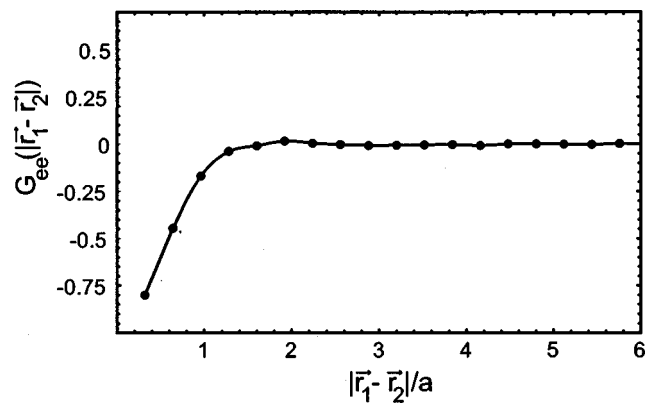


FIG. 2. Electron–electron correlation function, averaged from $t\omega_{pe} = 3.5$ to $t\omega_{pe} = 7.1$.

Indeed, the heating from three-body recombination is slightly larger than appears from this picture. The rate of increase in the electron temperature is reduced somewhat by collisional cooling on the ions (see Sec. II C). This effect is exacerbated by the artificially low mass ratio $m_i/m_e = 100$. By skipping ahead to Fig. 13, one can see the electron heating for the case of realistic mass ratio (for Xe ions), where the electron–ion collisional energy transfer is negligibly small over the duration of the simulation.

Figure 2 shows the electron–electron correlation function averaged over the time interval $t\omega_{pe} = 3.5$ to 7.1. The correlation function started out flat, corresponding to randomly distributed electrons, but quickly relaxed to the form shown in Fig. 2 and retained this form. The only change with increasing time was in the width of the region near $|\mathbf{r}_1 - \mathbf{r}_2| = 0$, where $G_{ee} \approx -1$. This value for G_{ee} reflects the fact that it is energetically unfavorable for two electrons to be at the same location, and the width of the region is of order $|\mathbf{r}_1 - \mathbf{r}_2| \approx e^2/kT_e$. In measurements of G_{ee} at later times the width was observed to decrease as the electron temperature slowly increased.

For comparison, Fig. 3 shows the correlation function for a one component plasma (OCP) in thermal equilibrium at correlation strengths $\Gamma = 1, 10, 20$, and 40.^{15,17} As expected, the correlation curve in Fig. 2 corresponds in shape to the $\Gamma = 1$ curve in Fig. 3. The curves in Fig. 3 for $\Gamma = 10, 20$, and

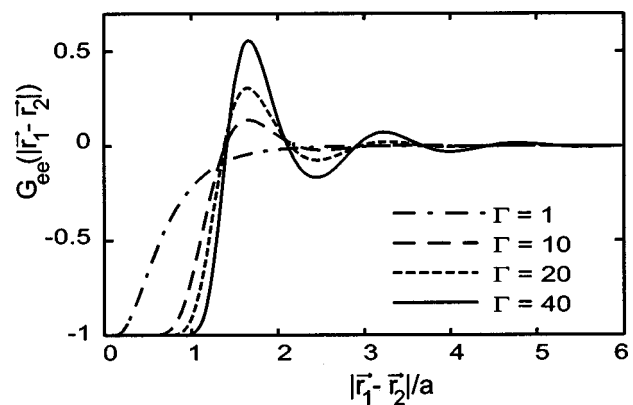


FIG. 3. Correlation function for one component plasma.

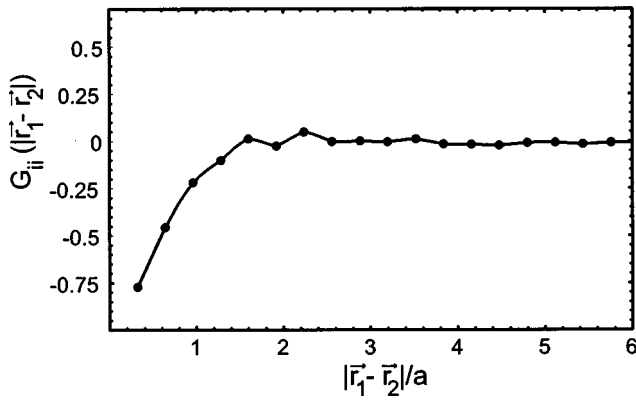


FIG. 4. Ion-ion correlation function averaged over the time interval $t\omega_{pe} = 67.4$ to $t\omega_{pe} = 70.9$.

40 exhibit oscillations indicating the presence of local order, that is, of a local lattice. The lack of these oscillations in Fig. 2 shows that such order was missing in the electron distribution for the ultracold plasma.

Figure 4 shows the ion-ion correlation function averaged over the time interval $t\omega_{pe} = 67.4$ – 70.9 . Again the correlation function started out flat and relaxed to the form shown, although the relaxation time was longer than for the electrons. The absence of oscillations shows that local order was missing.

Figure 5 shows the electron-ion correlation function averaged over the time interval $t\omega_{pe} = 3.5$ to 7.1 . In this case, G_{ei} is positive near $|\mathbf{r}_1 - \mathbf{r}_2| = 0$, since it is energetically favorable for an electron to be near an ion. However, this positive electron-ion correlation is not an indication of the local order characteristic of strong correlation; rather it reflects Debye shielding and the beginning of recombination. This latter observation also was made in Ref. 13.

Finally, we note that the experiments themselves provide some evidence against early strong correlation. The plasma expansion is driven by the electron pressure, but the effective pressure becomes negative for a strongly correlated plasma. This effect is well known from the theory of one component plasmas,¹⁷ and is easy to understand physically. Because of correlations, the electrostatic forces of interaction bind the

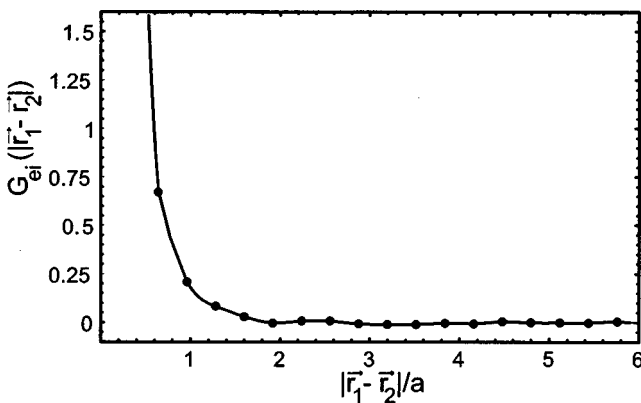


FIG. 5. Electron-ion correlation function averaged over the time interval $t\omega_{pe} = 3.5$ – 7.1 .

plasma together giving rise to an effective pressure that is negative. If there were no intrinsic heating and the cloud were strongly correlated, the pressure would be negative and the cloud would not expand. Alternatively, one can rule out expansion on energetic grounds. The correlation energy is negative [i.e., $U_{\text{corr}} \sim -N(e^2/a)$], so plasma expansion can occur only by supplying positive kinetic energy [i.e., $(3/2)NkT_e$]. However, in the limit of strong correlation, $\Gamma_e = e^2/akT_e \gg 1$, there is not enough kinetic energy to drive the expansion.

C. Ion-ion correlation in laser cooled clouds

Killian noted that both Strontium (Sr) atoms and Sr^+ ions can be laser cooled and suggested that a strongly correlated ion plasma might be achieved by laser cooling the ions shortly after the plasma is produced.⁷ We have explored this interesting suggestion using simulations.

The laser cooling was modeled in the simulations by periodically reducing the speed of each ion by a small percent. Two simulations were carried out: one for which the initial electron temperature was relatively high [i.e., $kT_e(0)/(e^2/a) = 1/\Gamma_e(0) = 31$] and another for which the initial temperature of both species was zero. For both simulations, 2048 electrons and 2048 ions were followed for the time $t_{\text{max}}\omega_{pe} = 354$, and total energy (plasma energy plus extracted energy) was conserved to better than $6 \times 10^{-4}Ne^2/a$. The mass ratio and the rounding parameter had the values $m_i/m_e = 100$ and $\varepsilon = 1/62$, and the particles initially were placed randomly inside a spherical volume bounded by a reflecting wall.

For the case of high initial electron temperature, Figs. 6(a) and 6(b) show the evolution of the ion and electron temperatures as a function of time. The ion temperature increased initially as ion-ion correlations develop and the correlation energy was released to heat the ions. The simulated laser cooling then reduced the ion temperature to a steady state value given by the balance between collisional heating from the electrons and ion cooling. Figure 6(b) shows that the electron temperature gradually decreased, as the electrons heated the ions. For the relatively high electron temperature in this simulation, three-body recombination and the concomitant heating of electrons was negligible.

Figure 7 shows the ion-ion correlation function averaged over the time interval $t\omega_{pe} = 106$ – 354 , which is the time interval of steady state ion temperature. The peak and the oscillations show the existence of order. Comparison to Fig. 3 for an OCP suggests a correlation strength in the range $\Gamma_i = 20$, which is in good agreement with the steady state ion temperature of Fig. 6(a) [i.e., $kT_i/(e^2/a) = 0.05$ or $\Gamma_i = 20$].

To see how the steady state ion temperature would scale with the electron to ion mass ratio and with the electron temperature, we note that weakly correlated electrons heat cold ions collisionally at the rate¹⁸

$$(\text{Heating})_{e,i} = \sqrt{32\pi} \frac{e^4 n}{\sqrt{m_e kT_e}} \frac{m_e}{m_i} \ln \left(\frac{\sqrt{3}}{\Gamma_e^{3/2}} \right). \quad (2)$$

Up to a numerical factor this expression is simply $\nu_{ei}(m_e/m_i)kT_e$, where ν_{ei} is the usual electron-ion collision

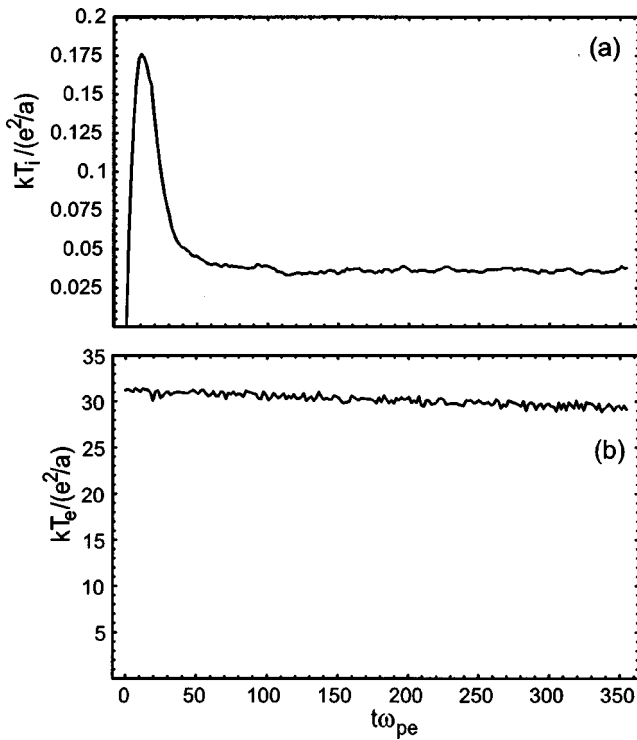


FIG. 6. Evolution of temperature as a function of time for the case of laser cooled ions and high initial electron temperature. (a) Ion temperature; (b) electron temperature.

frequency. If the laser cooling rate is given by $\gamma_i T_i$, then the steady state ion temperature is given by power balance,

$$\gamma_c T_i = \sqrt{32\pi} \frac{e^4 n}{\sqrt{m_e k T_e}} \frac{m_e}{m_i} \ln\left(\frac{\sqrt{3}}{\Gamma_e^{3/2}}\right). \quad (3)$$

The steady state ion temperature in Fig. 6(a) is given by this relation to within a factor of 2. To make T_i small, there is advantage in using heavy ions and hot electrons, although this latter advantage does not cut in until the scaled electron temperature $kT_e/(e^2/a) = 1/\Gamma_e$ exceeds about 10^3 . For scaled temperature between 1 and 10^3 , the $1/\sqrt{T_e}$ dependence and the $\ln(\sqrt{3}/\Gamma_e^{3/2})$ dependence compensate one another leaving the heating rate nearly independent of T_e .

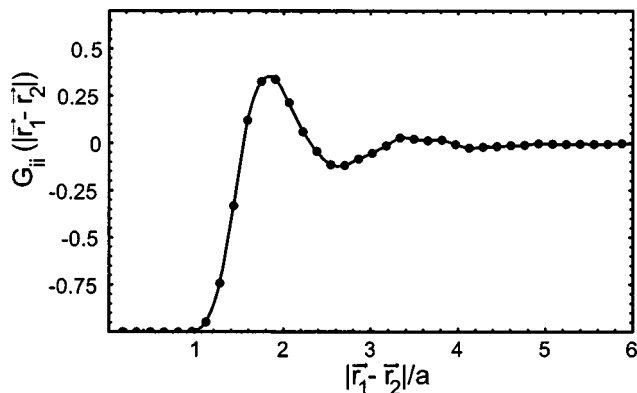


FIG. 7. Ion-ion correlation function averaged over time interval $t\omega_{pe} = 106$ to 354 for the case of laser-cooled ions and high initial electron temperature.

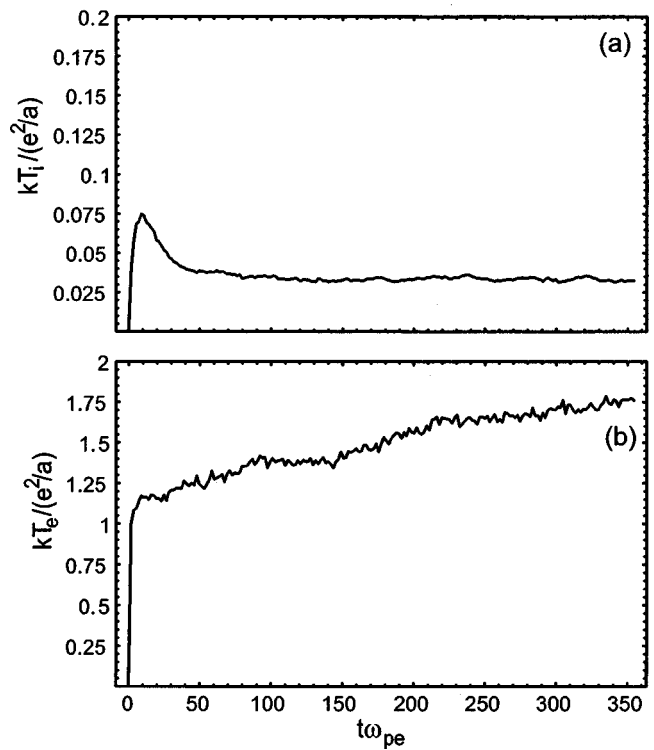


FIG. 8. Evolution of temperature as a function of time in the case of laser-cooled ions and zero initial electron temperature. (a) Ion temperature; (b) electron temperature.

More important reasons for using warm electrons are that the rate of three-body recombination is greatly reduced and the ion-ion interactions are not shielded. The reduction of the effective ion-ion coupling strength by electron shielding is illustrated by the simulations where both species were started with zero temperature. Figures 8(a) and 8(b) show the ion and electron temperature as a function of time. Initially both species are heated as correlation energy is released. Ion cooling then reduces the ion temperature to a steady state value that is in accord with Eq. (3). The electron temperature continues to rise gradually because heating due to three-body recombination exceeds collisional cooling on the ions.

Figure 9 shows the ion-ion correlation function aver-

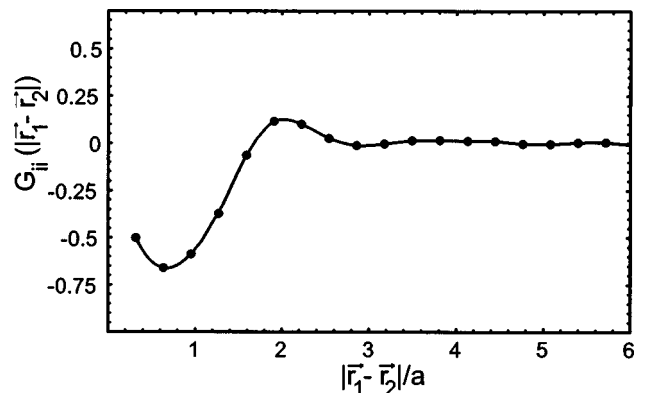


FIG. 9. Ion-ion correlation function averaged over the time interval $t\omega_{pe} = 106$ –354 for the case of laser-cooled ions and zero initial electron temperature.

aged over the time interval $t\omega_{pe}=106$ to 354. In this case, the evidence of order is less pronounced than for the previous simulation (see Fig. 7). Comparison to Fig. 3 for a OCP suggests a coupling parameter of $\Gamma_i < 10$, which is lower than that for the previous simulation, even though the two simulations have nearly the same steady state ion temperatures.

Presumably, the reason for the difference is that the electrons shielded the ion–ion interactions somewhat in the second simulation reducing the effective coupling strength. For weakly correlated electrons, the Debye shielded ion–ion interaction,

$$v = \frac{e^2}{r} \exp(-r/\lambda_D), \tag{4}$$

suggests an effective ion coupling strength $\Gamma'_i = \Gamma_i \exp(-a/\lambda_D)$.¹⁶ Here, $\lambda_D = (kT_e/4\pi n e^2)^{1/2}$ is the electron Debye length. The ratio $a/\lambda_D = \sqrt{3}\Gamma_e$ is small for hot electrons (i.e., $\Gamma_e \ll 1$), but is order unity for $\Gamma_e \sim 1$ implying a significant reduction in the effective correlation strength. For $\Gamma_e > 1$ the shielding is large but is not correctly described by expression (4).

Another interesting effect is apparent in Fig. 9. Note that $G_{ii}(|\mathbf{r}_1 - \mathbf{r}_2|/a)$ increases for $|\mathbf{r}_1 - \mathbf{r}_2|/a \lesssim 1$. We believe that weakly bound electron-ion pairs are polarized by and attracted to neighboring ions, and this causes $G_{ii}(|\mathbf{r}_1 - \mathbf{r}_2|/a)$ to turn upward at small $|\mathbf{r}_1 - \mathbf{r}_2|/a$. We checked this interpretation by removing ions with bound electrons from the sample used to evaluate G_{ii} , and found that G_{ii} goes to zero for $|\mathbf{r}_1 - \mathbf{r}_2|/a \lesssim 1$.

Apparently, the upturn occurs only for simulations where both the electrons and the ions are relatively cold. The electrons must be cold to have recombined pairs, and kT_i must be smaller than or comparable to the potential energy of interaction between the ion and the induced dipole. Note that the upturn does not occur in Fig. 7 or in Fig. 4.

III. THREE-BODY RECOMBINATION

A. Theory background

The traditional theory of three-body recombination, developed in a classic paper by Mansbach and Keck,⁸ yields the following expression for the recombination rate (per ion):

$$\mathcal{R} = 3.9 \times 10^{-9} \left[\frac{n}{\text{cm}^{-3}} \right]^2 \left[\frac{T_e}{\text{K}} \right]^{-9/2} \text{ s}^{-1}. \tag{5}$$

The predicted rate is very large at low temperature because of the scaling $T_e^{-9/2}$. However, the traditional theory assumes that $\Gamma_e < 1$, and rate expression (5) can be trusted only in this regime. Recently, Hahn¹⁹ extended the theory into the regime where $\Gamma_e > 1$.

For the highest density and lowest initial electron temperature reported in the experiments with ultracold plasma clouds, the initial value of Γ_e is larger than unity [i.e., $\Gamma_e(t=0) \approx 30$], so one might worry that the traditional theory would not be applicable. However, as we have seen, rapid initial heating reduces the value of Γ_e to unity or less. Thus, the experiments are on the edge of the range where the tra-

ditional theory is valid. The rate can be off by order unity, but not by the factor $(30)^{9/2}$ that one might have expected.

A deeper understanding of rate expression (5) requires an understanding of the kinetic bottleneck. To this end, consider a single ion at rest in a sea of electrons (neutralized by a uniform background charge). Suppose further that the Coulomb potential well for the ion is made flat at some relatively deep potential (below the bottleneck). When the system is in a state of thermal equilibrium, electrons are constantly going into and out of the well. The bottleneck can be understood by calculating the one way thermal equilibrium flux toward deeper binding. Using the Gibbs distribution and insight gained from a Monte Carlo analysis, Mansbach and Keck⁸ argued that the flux through a phase space surface characterized by binding energy E is proportional to

$$(\text{Flux})_1 \sim \frac{1}{E^4} \exp[-E/kT_e]. \tag{6}$$

The flux is the product of a phase space factor $1/E^4$ and a Boltzmann factor. For small values of $-E/kT_e$ the flux is large because the phase space factor, $1/E^4$, is large. For large $-E/kT_e$, the flux is large because the Boltzmann factor is large. The minimum at $E = -4kT_e$ is the kinetic bottleneck.

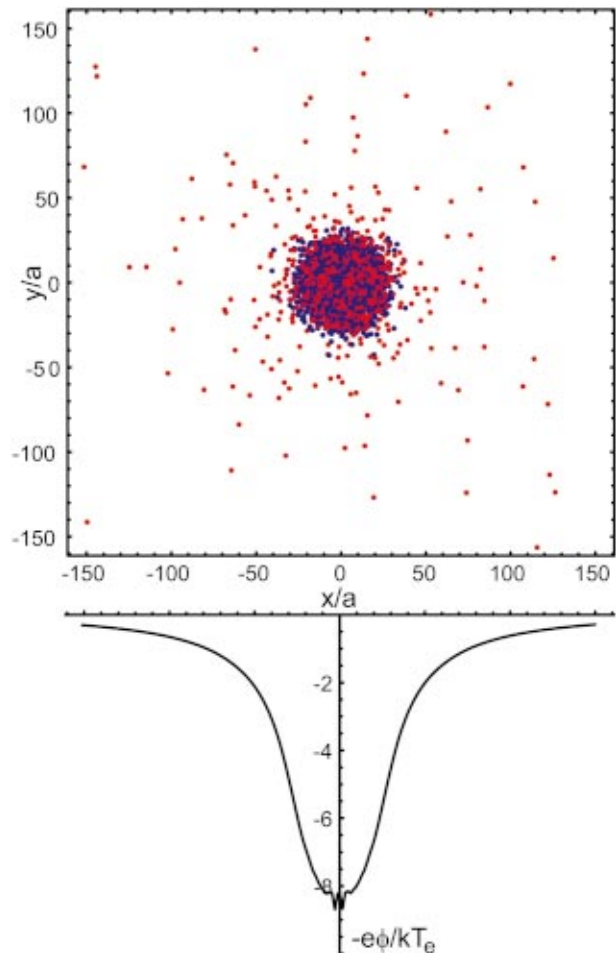


FIG. 10. (Color) Cloud at the end of the run, $t\omega_{pe}=354$; red dots are electrons and blue dots are ions. Part of the halo consists of suprathermal electrons that were produced as a by-product of three-body recombination. Also shown is a plot of the potential in the cloud at the end of the run.

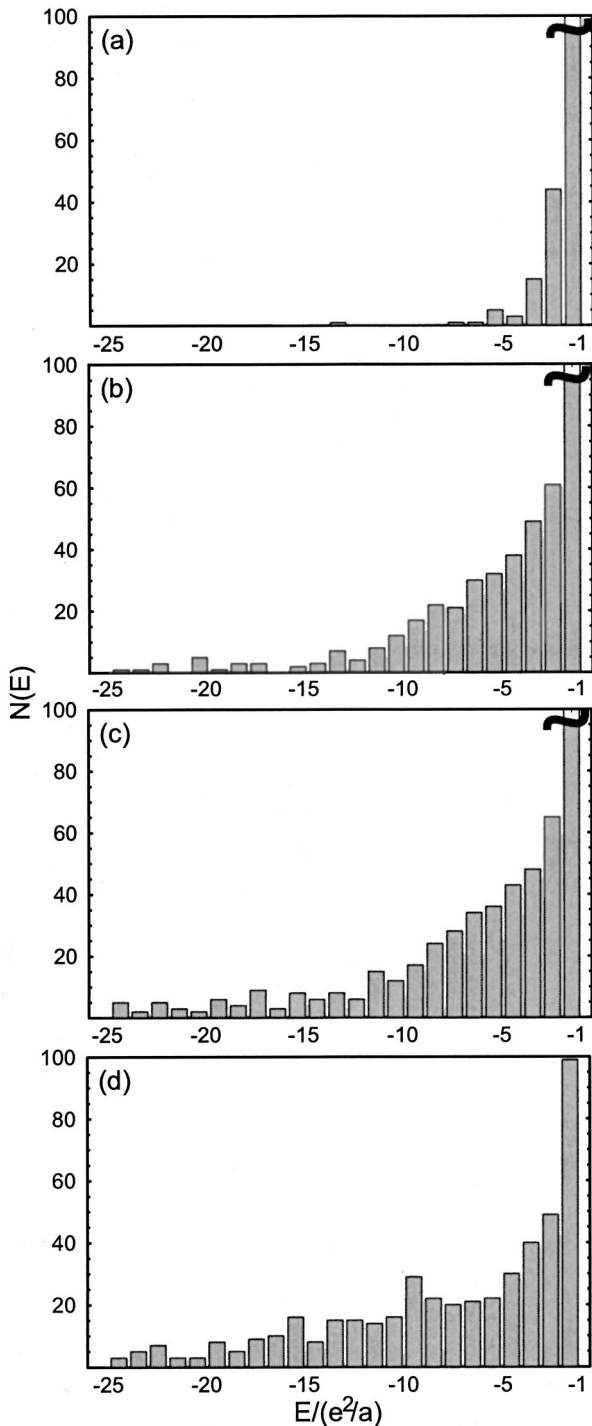


FIG. 11. Binding energy histograms at (a) $t\omega_{pe}=0$, (b) $t\omega_{pe}=117$, (c) $t\omega_{pe}=234$, (d) $t\omega_{pe}=354$. Each column shows the number of electrons in that energy bin. The squiggle at the top of the column for the lowest energy bin indicates that the number exceeds the range of the graph.

Electrons come into and out of the well many times before passing through the bottleneck. However, once they have fallen below the bottleneck, they continue to ever deeper binding. With this picture in mind, note that expression (5) is an evaluation of the one way flux through the bottleneck.

The reason that a collision almost always removes energy from a deeply bound pair can be understood dynamically. Consider an electron-ion pair with binding energy

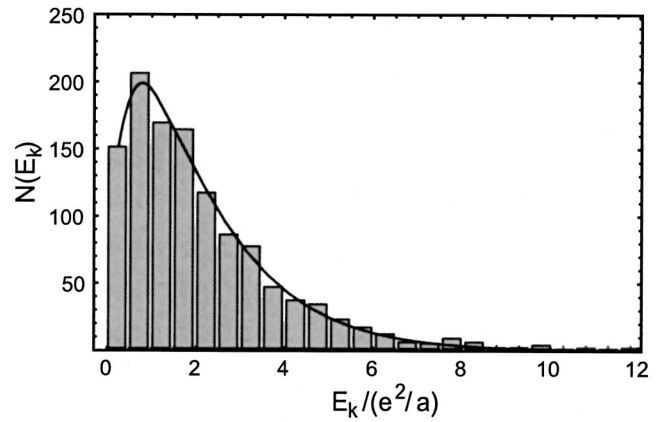


FIG. 12. Histogram of scaled kinetic energy for unbound electrons and a fit to a Maxwellian.

$|E| \gg kT_e$. On the average, the kinetic energy of the bound electron also is $|E|$. Consider a close collision with an electron that approaches with kinetic energy kT_e . Typically the collisional dynamics divides the kinetic energy more or less evenly between the two electrons, so one of the two leaves with energy $|E|/2 \gg kT_e$. The remaining electron is then bound more deeply. Incidentally, this simple picture shows how suprathermal electrons are produced as a by-product of the cascade to deeper binding.

B. Simulation results

Our most extensive simulation was used to study three-body recombination. The evolution of 4096 electrons and 4096 ions was followed for a scaled time $t_{max} \omega_{pe} = 354$, which required a month run on an XP-1000 alpha workstation. Energy was conserved to $2 \times 10^{-4} Ne^2/a$.

For this simulation, a realistic mass ratio was used (for Xe^+ ions), and the electrons and ions were distributed initially with a Gaussian density profile in accord with experiment. In scaled units, the mean-square radius of the Gaussian is specified by the number of electrons through $\langle r^2 \rangle / a^2 = (6/\pi)^{1/3} N^{2/3}$. In potential (1), the rounding parameter was chosen to have the value $\epsilon = 1/62$, which is small enough that the recombination dynamics (passage through the bottleneck) was treated accurately. Specifically, the inverse $1/\epsilon$

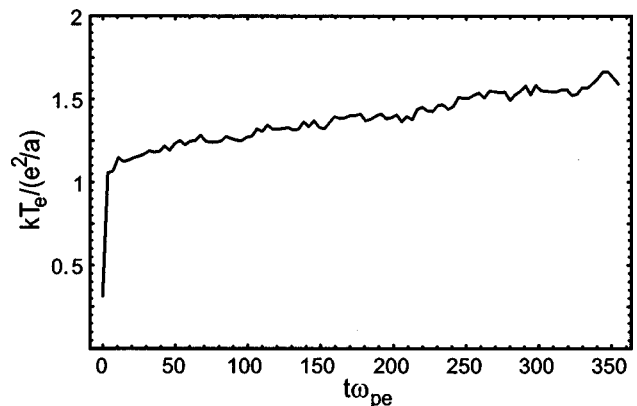


FIG. 13. Evolution of temperature in the cloud vs time.

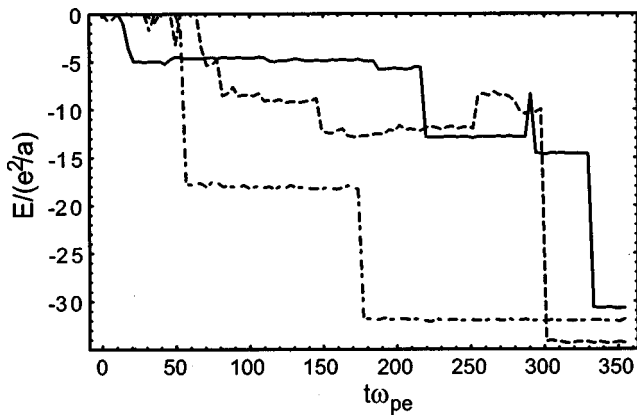


FIG. 14. Sample energy cascades to deeper binding.

$=62$ is much larger than the scaled binding energy at the bottleneck [i.e., $-E_b/(e^2/a) = 4/\Gamma_e \approx 7$]. Since $1/\epsilon = 62$ is comparable to the scaled binding energy of the most tightly bound pairs at the end of the simulation, the cascade rate to deeper binding for these pairs may have been slightly suppressed. Since the focus of this simulation is three-body recombination, rather than the rapid initial heating, the simulation started with a small but finite initial electron temperature [i.e., $kT_e/(e^2/a) = 1/\Gamma_e = 0.31$].

Figure 10 shows a picture of the cloud (red dots are electrons and blue dots are ions) at the end of the run. Many of the electrons in the surrounding halo were ejected from the cloud as suprathermal electrons produced as a by-product of three-body recombination.

Figures 11(a), 11(b), 11(c), and 11(d) show binding energy histograms for the four times $t\omega_{pe} = 0, 117, 234,$ and 354 . For a bound electron, the binding energy is the kinetic energy plus the potential energy in the field of the nearest ion. Each figure displays the number of particles in bins of scaled binding energy ranging from $E/(e^2/a) = -1$ to -25 . One can see the temporal progression to deeper binding.

Although the bound electrons were far from thermal equilibrium, the unbound electrons were nearly in thermal equilibrium. Figure 12 shows a histogram of scaled kinetic energy for unbound electrons and a fit to a Maxwellian. The

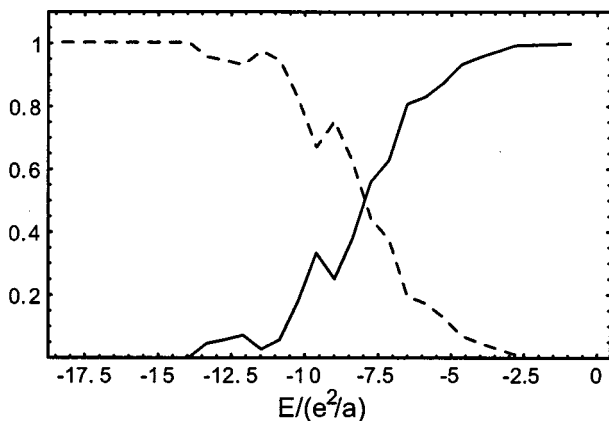


FIG. 15. The solid curve is the fraction of bound pairs that reached a given binding energy E , and then were reionized. The dashed curve is the fraction that made it from energy E to a sink at $E = -18e^2/a$. These two curves provide evidence for the existence of the bottleneck.

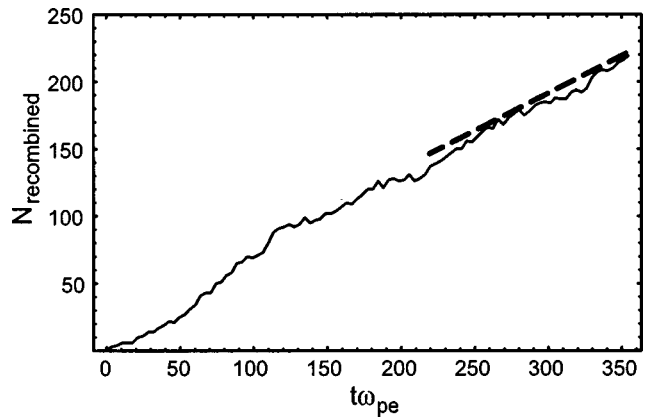


FIG. 16. Number of recombined pairs in the central region of the cloud.

fit determines the temperature of the unbound electrons at a particular time. Figure 13 shows the evolution of the temperature versus time. The gradual heating due to three-body recombination is apparent.

Figure 14 shows sample energy cascades to deeper binding. Each curve is a plot of scaled binding energy vs scaled time for an ion and bound electron, or sequence of electrons, since collisions can interchange bound and free electrons.

Figure 15 provides evidence for the existence of the bottleneck. The solid curve is the fraction of bound pairs that reached a given binding energy, E , and then were reionized. The dashed curve is the fraction that made it from energy E

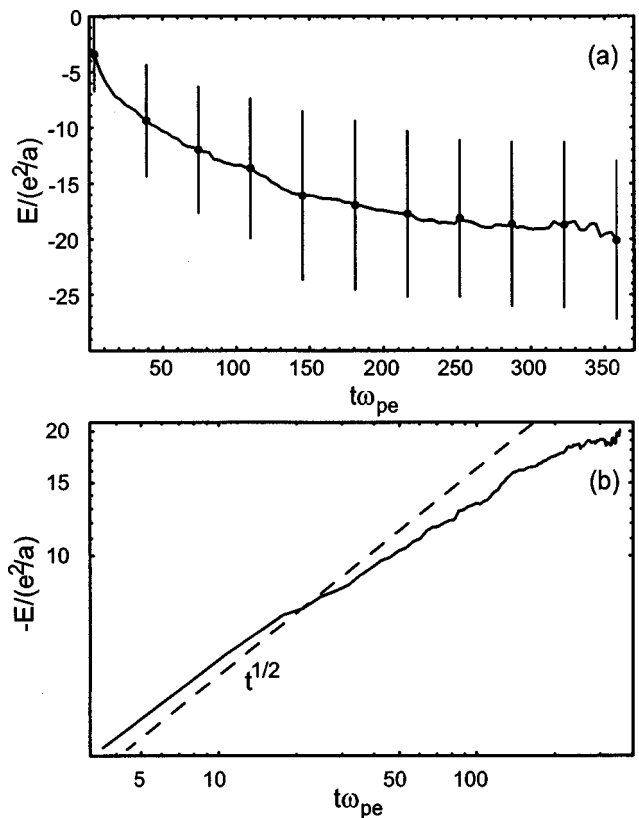


FIG. 17. (a) Average energy of an electron as it cascades to deeper binding. Error bars show the standard deviation for the distribution. (b) Log-log plot of the average energy.

to a sink at $E = -18(e^2/a)$. Taking the crossing point for the curves as the energy of the bottleneck yields $-E_b/(e^2/a) \approx 8$, which is close to four times the final temperature in Fig. 11 [i.e., $4T_e/(e^2/a) \approx 7$].

Figure 16 shows the number of recombined pairs in the central region of the cloud (i.e., for $r < r_p$) vs scaled time. Here, $r_p = \sqrt{2/3} \langle r^2 \rangle^{1/2}$ is the radius where the density has fallen to $1/e$ of its maximum value. Recall that a pair is defined to be recombined when its binding energy drops below the energy level of the bottleneck, which in accord with Fig. 15 we take to be $E_b = -8(e^2/a)$.

The dashed line at the top end of Fig. 16 provides a smoothed slope for $N_{\text{rec}}(t\omega_{pe})$ at the end of the run. From this slope we obtain the recombination rate for the particles in the central region, $dN_{\text{rec}}/dt \approx (0.56)\omega_{pe}$. For comparison the theoretical prediction from Eq. (5) for this rate is

$$\int_0^{r_p} 4\pi r^2 dr n \mathcal{R}(r, T) = (1.09)\omega_{pe}, \quad (7)$$

where $n(r)$ is the density of unrecombined ions in the central region and the scaled electron temperature $1/\Gamma_e = kT_e/(e^2/a) = 1.7$ has been used. Presumably, the factor of 2 difference between the predicted and observed rates is due to the fact that Γ_e is only slightly less than unity.

The solid curve in Fig. 17(a) shows the average energy of an electron as it cascades to deeper binding vs the time since initial binding. The average was constructed using the collection of bound pairs that ultimately reached the sink at $E/(e^2/a) = -12$, and the error bars show the standard deviation for the distribution. Figure 17(b) is a log-log plot of the curve, showing that the average binding energy increased like $t^{1/2}$.

This result is easy to understand physically. Consider an electron-ion pair bound with energy $|E| \gg kT_e$. Typically the kinetic energy and the potential energy of the electron are of order $|E|$, and the separation between the electron and ion is of order $d \sim e^2/|E|$. The frequency at which other electrons approach the pair within distance d is of order $\nu \sim n\bar{v}_e d^2$. In such a collision the two electrons typically share their kinetic energy. One electron leaves the collision with kinetic energy of order $|E| \gg kT_e$, and the binding energy of the remaining electron increases by order $|E|$. Thus, the rate of increase in the binding energy is approximately

$$\frac{d|E|}{dt} \sim \nu |E| = n\bar{v}_e \pi \frac{e^4}{|E|}. \quad (8)$$

To the extent that $n\bar{v}_e$ is approximately constant, we find that the binding energy increases with time as

$$|E| \sim [C + n\bar{v}_e \pi e^4 t/2]^{1/2}, \quad (9)$$

which agrees with the $t^{1/2}$ scaling in Fig. 17(b).

These ideas shed light on a recent experimental observation made with the ultracold plasma clouds.³ The number of

recombined pairs was observed to be a decreasing function of principle quantum number. Equivalently, the distribution over the magnitude of the binding energy, $N(|E|)$, was observed to be increasing in $|E|$ over a certain range below the bottleneck. For the histograms shown in Fig. 11 this is not the case. However, we believe that $dN/d|E|$ would become positive over some range if the simulations were run longer.

The reason is easy to understand physically. In steady state, the flux of bound pairs through any energy $|E|$ must be independent of $|E|$, so we obtain the equation

$$N(|E|) \frac{d|E|}{dt} (|E|) = \text{const.} \quad (10)$$

Since $d|E|/dt \propto 1/|E|$ decreases with increasing $|E|$, $N(|E|)$ must increase.

ACKNOWLEDGMENTS

The authors wish to thank Professor J. Kuti for suggesting the Aarseth simulation method and Professor T. Killian and Professor P. Gould for useful discussions.

This research was supported by National Science Foundation Grant No. PHY9876999 and Office of Naval Research Grant No. N00014-96-1-0239.

- ¹T. C. Killian, S. Kulin, S. D. Bergeson, L. A. Orozco, C. Orzel, and S. L. Rolston, *Phys. Rev. Lett.* **83**, 4776 (1999).
- ²S. Kulin, T. C. Killian, S. D. Bergeson, and S. L. Rolston, *Phys. Rev. Lett.* **85**, 318 (2000).
- ³T. C. Killian, M. Lim, S. Kulin, S. D. Bergeson, and S. L. Rolston, *Phys. Rev. Lett.* **86**, 3759 (2001).
- ⁴M. P. Robinson, B. L. Tolra, M. W. Noel, T. F. Gallagher, and P. Pillet, *Phys. Rev. Lett.* **85**, 4466 (2000).
- ⁵P. Gould and E. Eyster, *Phys. World* **14**, 19 (2001).
- ⁶S. K. Dutta, D. Feldbaum, A. Walz-Flannigan, J. R. Guest, and G. Raithel, *Phys. Rev. Lett.* **86**, 3993 (2001).
- ⁷T. C. Killian (private communication, 2001).
- ⁸P. Mansbach and J. Keck, *Phys. Rev.* **181**, 275 (1969).
- ⁹G. Zwicknagel, D. Klakow, P. G. Reinhard, and C. Toepffer, *Contrib. Plasma Phys.* **33**, 395 (1993).
- ¹⁰S. J. Aarseth, "Direct methods for N -body simulations," in *Multiple Time Scales*, edited by J. U. Brackbill and B. I. Cohen (Academic, New York, 1985), p. 377; J. Makino and S. J. Aarseth, *Publ. Astron. Soc. Jpn.* **44**, 141 (1992).
- ¹¹G. D. Quinlan, *New Astron.* **1**, 35 (1996).
- ¹²F. A. Rasio, J. M. Fregeau, and K. J. Joshi, "Binaries and globular cluster dynamics," in *The Influence of Binaries on Stellar Population Studies*, edited by D. Vanbeveren (Kluwer Academic, Dordrecht, 2001).
- ¹³S. Mazevet, L. A. Collins, and J. D. Kress, *Phys. Rev. Lett.* **88**, 055001 (2002).
- ¹⁴F. Robicheaux and J. D. Hansen, *Phys. Rev. Lett.* **88**, 055002 (2002).
- ¹⁵S. Ichimaru, *Rev. Mod. Phys.* **54**, 1017 (1982).
- ¹⁶M. S. Murillo, *Phys. Rev. Lett.* **87**, 115003 (2001).
- ¹⁷D. H. E. Dubin and T. M. O'Neil, *Rev. Mod. Phys.* **71**, 87 (1999).
- ¹⁸D. V. Sivukhin, "Coulomb collisions in a fully ionized plasma," in *Reviews of Plasma Physics* (Consultants Bureau, New York, 1966), Vol. 4, p. 138.
- ¹⁹Y. K. Hahn, *Phys. Lett. A* **231**, 82 (1997).